Nanoscale

ROYAL SOCIETY OF CHEMISTRY

PAPER

View Article Online
View Journal | View Issue

Cite this: *Nanoscale*, 2025, **17**, 4082

Oral delivery of MOMIPP lipid nanoparticles for methuosis-induced cancer chemotherapy†

Zeyuan Mao [a] and Guihong Chai *[a,b]

Methuosis, a non-apoptotic pattern of cell death, triggers the accumulation of macropinosome-derived vacuoles in the cytoplasm. Through this novel mechanism, methuosis inducers possess great potential in fighting apoptosis-resistant cancer cells and offer a promising alternative for cancer treatment. However, the potent methuosis inducer, 3-(5-methoxy, 2-methyl-1*H*-indol-3-yl)-1-(4-pyridinyl)-2-propen-1-one (MOMIPP), faces an intractable issue of insolubility in most solvents, hindering *in vivo* dosing and compromising the validation of its antitumor efficacy. Few strategies have been developed to effectively deliver MOMIPP and achieve robust *in vivo* tumor inhibition since its first report in 2012. Here, a MOMIPP self-emulsifying drug delivery system (MOMIPP-SEDDS) was developed to substantially improve its oral bioavailability and achieve a favorable antitumor effect in a mouse xenograft tumor model. Our findings demonstrated that the MOMIPP-SEDDS was internalized into Caco-2 cells *via* the lipid raft/caveolae pathway and exhibited enhanced absorption in both cell monolayers and everted gut sacs. Compared with MOMIPP suspensions, MOMIPP-SEDDS showed a 13.3-fold increase in peak concentration and increased relative bioavailability by 19.98 times. By inducing methuosis, MOMIPP-SEDDS successfully retarded tumor progression in a subcutaneous HeLa mouse tumor model. Additionally, transmission electron microscopy (TEM) images of the tumor sections evidenced the occurrence of methuosis in the MOMIPP-SEDDS treatment group. This MOMIPP-SEDDS emerges as a promising lipid nanoparticle platform and high translational medicine for the oral delivery of MOMIPP to exert methuosis-induced tumor suppression for cancer treatment.

Received 1st October 2024,
Accepted 20th December 2024

DOI: 10.1039/d4nr04044a

rsc.li/nanoscale

1. Introduction

Among the several means of anticancer treatment at present, chemotherapy still holds an irreplaceable position in clinical practice. However, the pro-apoptotic mechanisms exerted by classic anticancer drugs on tumor cells are prone to develop gene mutations.[1,2] Unfortunately, genomic instability is enhanced under the selective therapeutic pressure of conventional chemotherapy, causing drug resistance and attenuating the anti-tumor effects.[3,4] Clinically, the acquired drug resistance usually leads to the regrowth of tumors, which may involve mutations in drug targets, alterations in pathways, or histological changes.[4] Therefore, finding an alternative pathway to induce cancer cell death is of great importance to circumvent the impact of apoptosis-related gene mutations, overcome the existing drug resistance, and provide a potential solution to treat refractory tumors.

Methuosis, identified for the first time in glioblastoma cells ectopically expressing activated Ras, is a caspase-independent pattern of cell death.[5] Methuosis triggers cell death through a novel non-apoptotic mechanism, which cannot be salvaged by caspase inhibitors such as zVAD-fmk.[6] In the course of methuosis, the macropinosomes fail to fuse with lysosomes and merge to form large vacuoles in the cytoplasm, followed by a decrease in cell metabolic activities, rupture of the cell membrane, and eventual cell death. The indole-based chalcone, 3-(5-methoxy, 2-methyl-1*H*-indol-3-yl)-1-(4-pyridinyl)-2-propen-1-one (MOMIPP), induces methuosis in several cancer cell lines.[5] On the one hand, MOMIPP binds the vacuolization-related molecule target, PIKfyve (phosphatidylinositol-3-phosphate 5-kinase), and inhibits the PIKfyve kinase activity.[7] Upon exposure to MOMIPP for 4 h, endolysosomal trafficking is blocked and extreme vacuolization ensues.[8,9] On the other hand, MOMIPP disrupts glucose uptake and metabolism while activating the JNK1/2 stress kinase pathway.[9] Although the disruption of cell metabolism might not be the decisive factor causing cancer cell death, the multi-site phosphorylation of Bcl-2 (T56, S70, T74, S87) and the phosphorylation of Bcl-xL by

[a]*School of Pharmaceutical Sciences, Sun Yat-sen University, Guangzhou, 510006, China. E-mail: chaigh@mail.sysu.edu.cn*
[b]*State Key Laboratory of Anti-Infective Drug Discovery and Development, School of Pharmaceutical Sciences, Sun Yat-sen University, Guangzhou, 51006, China*
† Electronic supplementary information (ESI) available. See DOI: https://doi.org/10.1039/d4nr04044a

the JNK signaling axis, disrupting their pro-survival functions, are considered crucial steps in triggering the cytotoxic effects of methuosis. With the ability to induce methuosis, MOMIPP is considered a potential candidate for cancer treatment, especially in cases resistant to conventional apoptosis. Notably, MOMIPP has been reported to induce methuosis and cause a dramatic decrease in cell viability in temozolomide (TMZ)-resistant U251 glioblastoma cells and doxorubicin (Dox)-resistant MCF-7 breast cancer cells.[5] Due to its specific cytotoxic effects on cancer cells, MOMIPP has great potential for combating apoptosis-resistant tumors. Nevertheless, the poor solubility of MOMIPP poses a serious challenge, as seen in other hydrophobic anticancer drugs. It has been reported that the solubility of MOMIPP in water is merely 0.003 ± 0.0003 mg mL^{-1}, and 0.651 ± 0.019 mg mL^{-1} in ethanol.[10] The poor solubility in water and common organic solvents makes its administration *in vivo* extremely difficult. In a former study, the MOMIPP suspension showed disappointing pharmacokinetic performance, where MOMIPP in the plasma dropped below the detectable level within 2 h with a plasma half-life of 0.4 h.[10] Additionally, the *in vivo* efficacy of MOMIPP suspension was hindered by the poor solubility and dissolution rate in the gastrointestinal tract, greatly attenuating its antitumor activity.[11] To date, few publications have reported successfully delivering this promising compound *in vivo*.[9,10,12] One efficient delivery approach was *via* intraperitoneal injection, which only demonstrated moderate therapeutic effects (p = 0.036).[9] Another approach was *via* intravenous injection, which showed increased drug accumulation at tumor sites, but the antitumor efficacy was validated by intratumoral injection, which may be attributed to the still insufficient delivery of MOMIPP to the tumor sites.[12] Hence, there is an urgent need for an effective delivery system for MOMIPP to improve its bioavailability and tumor site delivery efficiency to verify its methuosis-mediated anti-tumor efficacy *in vivo*.

Compared to injection routes, oral administration is an attractive alternative with excellent patient convenience, self-administration capacity, and treatment flexibility.[13] A self-emulsifying drug delivery system (SEDDS), consisting of a drug, oil, surfactant, and co-surfactant, is a promising approach to orally delivering hydrophobic drugs.[14,15] Under mild agitation in gastrointestinal aqueous fluid, SEDDS spontaneously forms a nano-sized oil-in-water emulsion. Furthermore, surfactants used as excipients endow SEDDS with mucus-permeating ability, allowing access to the underlying epithelial cells,[16] as reported in several studies.[17,18] Additionally, upon the lipolysis of the lipids in SEDDS, fatty acids, monoglycerides, and bile salts form drug-loaded mixed micelles.[19,20] These micelles bind with chylomicrons and can be transported *via* the lymphatic system.[19,21] Through this process, the drug can directly enter blood circulation, bypassing the first-pass effect.

Since no effective oral dosage form designed for MOMIPP has been explored, utilizing oral SEDDS for the delivery of MOMIPP could provide an important complement to this field. In this study, an oral MOMIPP-loaded SEDDS (MOMIPP-SEDDS) with significantly improved pharmacokinetics and pharmacodynamics was developed for cancer chemotherapy. To achieve this, the optimized formulation of MOMIPP-SEDDS was screened with the aid of Design of Experiment, achieving a remarkably increased solubility of MOMIPP to 5.361 mg g^{-1} in the preconcentrate. Upon self-emulsification, MOMIPP-SEDDS exhibited a unique superiority in absorption improvement both *in vitro* and *in vivo*. Furthermore, this MOMIPP-SEDDS demonstrated an appealing antitumor effect, effectively shrinking the tumor volume and reducing the tumor weight.

2. Materials and methods

2.1. Materials

Maisine® CC (glyceryl monolinoleate), Transcutol® HP (diethylene glycol monoethyl ether), Peceol™ (glyceryl monooleate), Labrafac™ MC60 (glyceryl monocaprylocaprate), and Labrafil® M 1944 CS (oleoyl macrogol-6 glycerides) were kindly provided by Gattefossé (Saint-Priest, France). Kollisolv® MCT 70 (medium chain triglycerides), Kolliphor® RH 40 (macrogol-glycerol hydroxystearate), and Kolliphor® ELP (polyoxyl 35 castor oil) were gifted from BASF (Ludwigshafen, Germany). Oleic acid, castor oil, corn oil, and coumarin 6 (Cou-6) were purchased from Aladdin (Shanghai, China). Tween 80 was obtained from Sigma-Aldrich (St Louis, USA). Thiazole blue (MTT) was purchased from Merck KGaA (Darmstadt, Germany). Hoechst 33342 was sourced from Invitrogen (Eugene, USA). Krebs–Ringer (K–R) bicarbonate solution was purchased from Leagene (Beijing, China). Dulbecco's modified Eagle's medium (DMEM), fetal bovine serum (FBS), nonessential amino acids, penicillin, streptomycin, 0.25% trypsin–EDTA solution, phosphate buffered saline (PBS), and Hanks' balanced salt solution (HBSS) were all purchased from Gibco BRL (USA). MOMIPP was synthesized according to the method reported by Robinson MW *et al*.[5] Other reagents were of analytical or chromatographic grade.

2.2. Cell lines and animals

Caco-2 cells and MDCK cells were purchased from the Institute of Biochemistry and Cell Biology (Shanghai, China) and cultured in DMEM supplemented with 10% (v/v) FBS, 1% (v/v) penicillin–streptomycin, and 1% (v/v) nonessential amino acids. The HeLa cell line was purchased from the American Type Culture Collection (ATCC) and cultured in RPMI-1640 supplemented with 10% (v/v) FBS and 1% (v/v) penicillin–streptomycin.

Healthy Sprague-Dawley (SD) male rats (180–220 g), SD female rats (230–270 g), and Balb/c-nu female mice (4–6 weeks) were obtained from the Laboratory Animal Center of Sun Yat-sen University (Guangzhou, China). All animal experiments were conducted according to the protocols approved by the Institutional Animal Care and Use Committee of Sun Yat-sen University (2023002636, 2023003046). The animals were housed in an SPF barrier environment with a temperature of 20–26 °C and humidity of 40–70%, under a 12 h/12 h dark/light cycle.

2.3. MOMIPP solubility measurement

To maximize the solubility of MOMIPP in the excipients of SEDDS, various oil phases, surfactants, and co-surfactants commonly used for SEDDS preparation were screened. In brief, an excess amount of MOMIPP was added to the excipients, and then the mixture was treated with ultrasound for 10 min and vortexed evenly, followed by shaking in an air bath at 37 °C for 24 h. The samples were centrifuged at 10 000*g* for 10 min and the supernatant was diluted with a suitable amount of dimethyl sulfoxide (DMSO) for further quantification of MOMIPP using high performance liquid chromatography (HPLC). The quantification of MOMIPP was performed on a Shimadzu Prominence-i HPLC system, under the following conditions: column, Welch Ultimate® XB-C18 (5 μm, 4.6 × 250 mm); flow rate, 1 mL min^{-1}; eluents, 50% water and 50% acetonitrile; column temperature, 40 °C; detection wavelength, 419 nm; injection volume, 20 μL.

2.4. Construction of ternary phase diagrams

Based on the solubility results of MOMIPP, Maisine® CC, RH 40, and Transcutol® HP were chosen as oil, surfactant, and co-surfactant, respectively. The oil, surfactant, and co-surfactant were mixed to form SEDDS preconcentrates varying in proportions with different K and K_m values. Subsequently, the preconcentrate was diluted 1 : 100 (v/v) with water at 37 °C and magnetically stirred gently (100 rpm).[22] The proportions of excipients that generated clear and transparent nano-sized emulsion within 1 minute were determined as the effective self-emulsifying regions in the ternary phase diagrams. Further investigation to optimize the formulation was performed within the scope of the self-emulsifying region.

2.5. Optimization of SEDDS formulation

The Mixture-Optimal (Custom) method in Design Expert 13 software was employed to optimize the ratio of oil, surfactant, and co-surfactant in the SEDDS formulation. The proportion of each excipient was set within the scope of the self-emulsifying region. The MOMIPP drug loading and the polydispersity index (PDI) of the self-emulsified nano-sized emulsion were chosen as indicators for the design. The components of the SEDDS preconcentrate were weighed and mixed according to the design table (Table S1†). The drug loading capacity was determined as described in the solubility studies. The preconcentrate (0.2 mL) was added to 20 mL of water at 37 °C under gentle stirring (100 rpm). When the preconcentrate dispersed and formed a clear solution, self-emulsification was achieved. Subsequently, the nano-sized emulsion was sampled to measure the droplet size and PDI using a Malvern Zetasizer Nano-ZS90 (Malvern Instruments, Worcestershire, UK).

2.6. Preparation and characterization of MOMIPP-SEDDS

The SEDDS preconcentrates were prepared by mixing oil, surfactant, and co-surfactant with/without the addition of MOMIPP. After the drug was completely dissolved, the preconcentrates were emulsified by the aforementioned method. Upon emulsification, the nano-sized emulsion was sampled and characterized using the Malvern Zetasizer Nano ZS90 in terms of droplet size, PDI, and zeta potential. The stability of MOMIPP-SEDDS was evaluated by measuring any drug precipitation within the time frame of intestinal transport.[23,24] The morphology of the nano-sized emulsion was examined by transmission electron microscopy (TEM, HT7800, Hitachi, Japan).

2.7. *In vitro* release profiles of MOMIPP-SEDDS and MOMIPP suspension

The *in vitro* drug release behavior of MOMIPP from its SEDDS and corresponding suspension (dispersed in 0.5% w/v carboxymethyl cellulose suspension containing 0.1% w/v Tween-80) was evaluated using a dialysis bag method, with PBS containing 2% sodium dodecyl sulfate (SDS) as the release medium. In brief, a sample of 1 mL emulsified MOMIPP-SEDDS or MOMIPP suspension (636.8 μg MOMIPP equivalent) was added to the dialysis bag, and the bag was placed in a centrifuge tube with 40 mL of release medium. The centrifuge tube was transferred to a thermostatic shaker at the rate of 60 rpm with the temperature maintained at 37 °C. Aliquots of 2 mL of the release medium were sampled at predetermined time intervals (0 min, 15 min, 30 min, 1 h, 2 h, 3 h, 5 h, 7 h, 9 h, 12 h, 24 h, 30 h, 36 h), and an equivalent volume of fresh release medium was immediately supplemented at the same time. The drug concentrations in the samples were determined using HPLC.

2.8. Storage stability studies

To investigate the storage stability of MOMIPP-SEDDS, the preconcentrates were stored at temperatures of 4 °C, 37 °C, and 50 °C for 30 days. At pre-determined intervals, the preconcentrates were sampled and diluted with DMSO to measure the drug content using HPLC. The emulsified MOMIPP-SEDDS was then evaluated for droplet size and PDI.

2.9. Cytotoxicity studies

The potential cytotoxicity of blank SEDDS against MDCK and Caco-2 cell lines was evaluated using the MTT assay. In brief, MDCK or Caco-2 cells were seeded in a 96-well plate at a density of 1×10^4 cells per well, and incubated for 24 h. The culture medium was then replaced with blank DMEM containing various concentrations of blank SEDDS (0.25%, 0.1%, 0.05%, 0.01%) and incubated for 24 h. Subsequently, 20 μL of MTT solution (5 mg mL^{-1} in PBS) was added, and the plate was incubated in darkness for another 4 h at 37 °C. Afterward, the medium was replaced with 200 μL of DMSO to dissolve the formazan crystals. After shaking the plate on an orbital shaker for 15 min, the optical density (OD) value of each well was measured at 490 nm using an automatic microplate reader (ELX800, Bio-Tek, USA). For the cytotoxicity investigation of the MOMIPP-SEDDS, the protocol was the same as mentioned above, except the cells were treated with MOMIPP-SEDDS at various MOMIPP concentrations (0, 5, 10, 50, 100, 200, and 400 μM) and the incubating time was 4 h.

Additionally, to investigate whether MOMIPP-SEDDS can cause vacuolization during intestinal absorption. Caco-2 cells were incubated with DMEM, blank SEDDS, MOMIPP-SEDDS (400 μM MOMIPP), and MOMIPP suspensions (400 μM MOMIPP) for 4 h and 6 h, respectively. Images were taken using optical microscopy to evaluate the vacuolization induction in the cytoplasm. The number of vacuolized cells was counted, and the vacuolization rate was calculated.

2.10. Cellular uptake and endocytosis mechanisms in Caco-2 cells

Fluorescence microscopy (EVOS M7000, Invitrogen, USA) and flow cytometry (CytoFLEX S, Beckman Coulter, USA) were employed to examine the cellular uptake of the SEDDS loaded with Cou-6 (COU-SEDDS) in Caco-2 cells. In brief, Caco-2 cells were seeded in a 12-well plate (2×10^4 cells per well for fluorescence microscopy and 1×10^5 cells per well for flow cytometry, respectively) and incubated for 24 h. Afterward, the cells were incubated with COU-SEDDS for different periods. At the end of the incubation, the cells were rinsed with cold PBS thrice. For fluorescence microscopy, the cells were fixed with 4% paraformaldehyde and the nuclei were stained by Hoechst 33342 (10 μg mL^{-1}). Fluorescence images of each field were captured with the same settings. For flow cytometry, the cells were harvested and analyzed using a flow cytometer. FlowJo was utilized for post-processing and analysis. The relative mean fluorescence intensity (RMFI), which indicates the average endocytosed COU-SEDDS per cell, was calculated using the equation below:

$$\mathrm{RMFI} = \frac{\mathrm{MFI(T)}}{\mathrm{MFI(C)}} - 1$$

where MFI(T) represents the mean fluorescence intensity of cells in the COU-SEDDS treated group and MFI(C) represents the mean fluorescence intensity of cells in the negative control group.

The endocytosis pathways of the SEDDS nanoemulsion in Caco-2 cells were investigated by incubating the cells with COU-SEDDS under different conditions. Caco-2 cells were pretreated with various endocytosis inhibitors, including genistein (50 μg mL^{-1}), methyl-β-cyclodextrin (M-β-CD, 5 mM), chlorpromazine (10 μg mL^{-1}), and 5-(*N*-ethyl-*N*-isopropyl) amiloride (EIPA) (10 μg mL^{-1}) for 30 min.[25] Subsequently, the cells were incubated with COU-SEDDS containing the corresponding endocytosis inhibitors at the same concentrations for another 2 h. Additionally, another parallel experiment on endocytosis was conducted at 4 °C to investigate any energy-dependent process. At the end of incubation, the cells were rinsed with PBS and stained with Hoechst 33342. Images were taken using a high-content imaging system (ImageXpress MicroConfocol, Molecular Devices, USA) and statistical analysis was conducted using MetaXpress software.

2.11. Transport of MOMIPP-SEDDS across Caco-2 and MDCK cell monolayers

Caco-2 or MDCK cells were seeded on polycarbonate membrane of Transwell inserts (24-well) with 0.4 μm membrane pore size (Corning, New York, USA) to establish cell monolayers. In brief, 0.1 mL of culture medium containing 2×10^4 cells was added to the upper compartment of each Transwell insert, and 0.5 mL of cell-free culture medium was added to the lower compartment. For Caco-2 cells, the medium was changed every 2 days in the first two weeks and every day in the third week. For MDCK cells, the medium was changed every 2 days for one week. The integrity of the cell monolayers was verified by measuring the transepithelial electrical resistance (TEER) value using a Millicell-ERS volt-ohmmeter. The Caco-2 cell monolayers with a TEER value exceeding 800 Ω cm^2 and the MDCK cell monolayers with a TEER value over 180 Ω cm^2 were selected for the subsequent transepithelial transport experiments.[26,27] For the transport experiment, the culture medium in the upper compartment was replaced with MOMIPP-SEDDS or MOMIPP suspensions (equivalent to 400 μM MOMIPP in HBSS), while the medium in the lower compartment was changed to blank HBSS. After 4 h of transport, the medium in both compartments was collected and an equivalent volume of DMSO was added for demulsification. Subsequently, the samples were centrifuged at 10 000*g* for 10 min, and the supernatant was used to quantify the amount of MOMIPP using HPLC.

2.12. Intestinal absorption of MOMIPP-SEDDS and MOMIPP suspensions by *ex vivo* everted gut sac

Male SD rats (200 ± 20 g) were fasted but had free access to water for 12 h before the experiments. After being euthanized by an intraperitoneal injection (IP) of an overdose of tribromoethanol, the abdominal cavity of the rat was opened to isolate the desired intestine segments. The excised segments were immediately washed with iced cold Krebs–Ringer (K–R) bicarbonate solution to clean the intestinal contents and everted with a smooth glass rod. The intestine was tied at one end, and the other was inserted with a plastic tube for sampling.[28,29] The serosa compartment (the receiver compartment) of the everted gut sac was filled with 1.3 mL of K–R solution and then immersed in 40 mL of K–R bicarbonate solution containing emulsified MOMIPP-SEDDS or MOMIPP suspensions (equivalent to 400 μM MOMIPP). During the absorption process, the solution was continually aerated with 5% CO_2 and 95% O_2, with the temperature maintained at 37 °C. Aliquots of 0.4 mL of the solution were sampled from the receiver compartment at different time intervals (0, 30, 60, 120 min), and supplemented with an equivalent volume of fresh K–R bicarbonate solution at the same time. At the end of the experiment, the length of the absorbing intestine segment was measured. To quantify the drug absorption, 200 μL of the samples were vortexed with 200 μL DMSO, centrifuged at 15 000 rpm for 20 min, and the supernatant was used to measure the amount of MOMIPP using HPLC. The absorption of MOMIPP per unit = the amount of MOMIPP absorbed (μg)/the length of the absorbing intestinal segment (cm).

2.13. *In vivo* pharmacokinetic studies

Female SD rats (250 ± 20 g) were fasted for 12 h with free access to water before the experiments. The animals were ran-

domly divided into two groups (n = 6): one group was given the MOMIPP-SEDDS (50 mg kg^{-1}, MOMIPP), and the other group was given the MOMIPP suspensions (50 mg kg^{-1}, MOMIPP). Orbital blood samples were collected at predetermined intervals and centrifuged at 5000g for 10 minutes immediately to collect the plasma. After being precipitated by methanol, the plasma was centrifuged at 12 000g for 10 minutes, and the supernatant was collected, filtered, and analyzed using a UPLC-MS/MS system (TSQ Quantum Access Max, Thermo Scientific, USA) equipped with an electrospray ionization (ESI) source. Chromatographic separation was performed using an Xterra MS C18 column (5 μm, 2.1 × 100 mm, Waters, Ireland) maintained at 40 °C with an injection volume of 10 μL. The isocratic elution method was as follows: 70% methanol and 30% water containing 0.1% formic acid with a flow rate of 0.25 mL min^{-1}. The quantification of MOMIPP was performed using multiple reaction monitoring (MRM) in positive ion mode with the following ionization conditions: spray voltage 3800 V, sheath gas pressure 45 psi, auxiliary gas pressure 15 bar, capillary temperature 300 °C, and collision energy 22 eV. The transition of the precursor ion to the product ion was 293.0/96.1 for MOMIPP. The scan time was set at 0.1 s with a scan width of 0.01 m/z. Nitrogen gas was used as the carrier gas, while argon gas used as the collision gas. The pharmacokinetic data were analyzed using DAS software.

2.14. *In vivo* antitumor studies

Balb/c-nu female mice (4–6 weeks) were subcutaneously injected with 2 × 10^6 HeLa cells into the right flank to establish the HeLa xenograft tumor model. When the size of the tumors reached 100–150 mm^3, the mice were randomly divided into four groups (n = 6), including orally administrated saline, MOMIPP suspensions (50 mg kg^{-1}, MOMIPP), blank SEDDS, and MOMIPP-SEDDS (50 mg kg^{-1}, MOMIPP). The mice were administrated once a day for 14 consecutive days during the treatment. The body weight and tumor volume were monitored throughout the study. The tumor volume was calculated using the following formula: tumor volume (mm^3) = 0.5 × length × width^2. When the treatment reached the endpoint, all the mice were euthanized to collect the major organs (heart, liver, spleen, lung, and kidney) and jejunum for histopathological examination by H&E staining. At the same time, the tumors were collected, weighed, and photographed. The tumor growth inhibition (TGI) rate was calculated using the formula below:

$$\mathrm{TGI}\,(\%) = \left(1 - \frac{\text{tumor weight}_{\text{test}}}{\text{tumor weight}_{\text{control}}}\right) \times 100,$$

where tumor weight$_{\text{test}}$ and tumor weight$_{\text{control}}$ represent the weight of tumors from the corresponding treatment group and the saline group.

A portion of the tumor tissue was fixed in 4% paraformaldehyde for Ki67 staining and examined using fluorescence microscopy (EVOS M7000, Invitrogen, USA). The other part of the tumor tissue was fixed in 2% glutaraldehyde, dehydrated, and embedded in resin. The ultrathin sections of tumor tissue were mounted on copper grids, impregnated with uranyl acetate and lead citrate, and examined under a transmission electron microscope (JEM-1400, JEOL, Japan).

2.15. Statistical analysis

The data are presented as the mean ± standard deviation (SD) from at least three independent tests. Statistical analysis was performed using Student's t-test or one-way ANOVA with GraphPad Prism 8, and statistical significance was assigned at $p < 0.05$. The corresponding symbols in the figures are defined as $^*p < 0.05$, $^{**}p < 0.01$, and $^{***}p < 0.001$ respectively.

3. Results

3.1. SEDDS formulation optimization

A self-emulsifying drug delivery system (SEDDS), comprising oil, surfactant, and co-surfactant, tends to form an oil-in-water (o/w) nano-sized emulsion upon encountering an aqueous phase with slight agitation.[14,30] Due to this unique feature, SEDDS has been widely used to deliver poorly water-soluble drugs. Various commonly used oils, surfactants, and co-surfactants were screened to optimize the SEDDS formulation with the maximum MOMIPP solubility and satisfactory physicochemical properties. Since MOMIPP is a highly water-insoluble compound and poorly soluble even in some pharmaceutically acceptable solvents, the capacity of excipients to dissolve MOMIPP was prioritized (Fig. 1). The SEDDS components, consisting of commonly used and generally recognized as safe excipients, with relatively high MOMIPP solubility were selected for formulation screening. Additionally, considering the need for a shorter emulsification time for improved efficiency, Maisine® CC, Kolliphor® RH 40, and Transcutol® HP were selected for further studies.

The ternary phase diagrams with various K_m values (the ratio of surfactant to co-surfactant) were constructed to determine the suitable proportion range of each excipient. A series of SEDDS preconcentrates were prepared and characterized for their self-emulsification behavior. Only the formulations

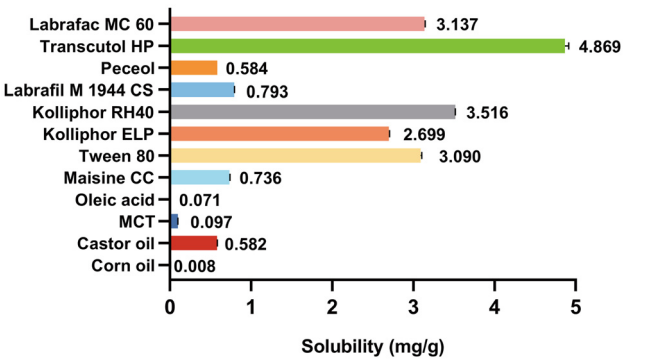

Fig. 1 Solubility of MOMIPP in various oil phases, surfactants, and co-surfactants.

forming clear and transparent nano-sized emulsions were regarded as effective SEDDS formulations. Accordingly, the composition proportion of effective formulations was marked in the ternary phase diagrams (Fig. 2A–F). Based on the ternary phase diagrams, the proportion range of oil was set within 0–20%, and the K_m value ranged from 7 : 3 to 5 : 5. Subsequently, the SEDDS formulation was further optimized using the Mixture-Optimal (Custom) module in Design Expert 13. The design and results of the experiments are shown in Table S1.† As the droplet size and the emulsification time of all tested samples showed almost no difference, the drug loading capacity and the PDI were taken as the indicators. The equations of the fitting model were successfully established, with the drug loading equation fitting the quadratic model and the PDI equation fitting the special quartic model (Table S2†). The coded equations are described as followed: drug loading = $2.39A + 4.91B + 6.07C + 1.18A \times B + 0.1817A \times C + 1.57B \times C$; PDI = $1.78A + 0.1278B + 0.1915C - 2.08A \times B - 2.41A \times C + 0.4571B \times C - 10A^2 \times B \times C + 6.26A \times B^2 \times C - 3.63A \times B \times C^2$. The contour map and 3D-effect surface map pertaining to these two indicators and the influences of the three components by Design Expert 13 are shown in Fig. 2G. By calculation with the equations, the optimal formulation was predicted as follows: Maisine® CC : RH 40 : Transcutol® HP = 0.1 : 0.429 : 0.471 (wt/wt/wt). The predicted drug loading was 5.096 mg g^{-1}, and the predicted PDI of the microemulsion was 0.108. According to the predicted optimal SEDDS formulation, the validation experiments were conducted. The measured drug loading was 5.361 mg g^{-1} and the PDI of the SEDDS emulsion was 0.112, which supported the predicted results of the mathematical models (Fig. 2H). Consequently, the optimal SEDDS formulation for MOMIPP was obtained and used in the later research.

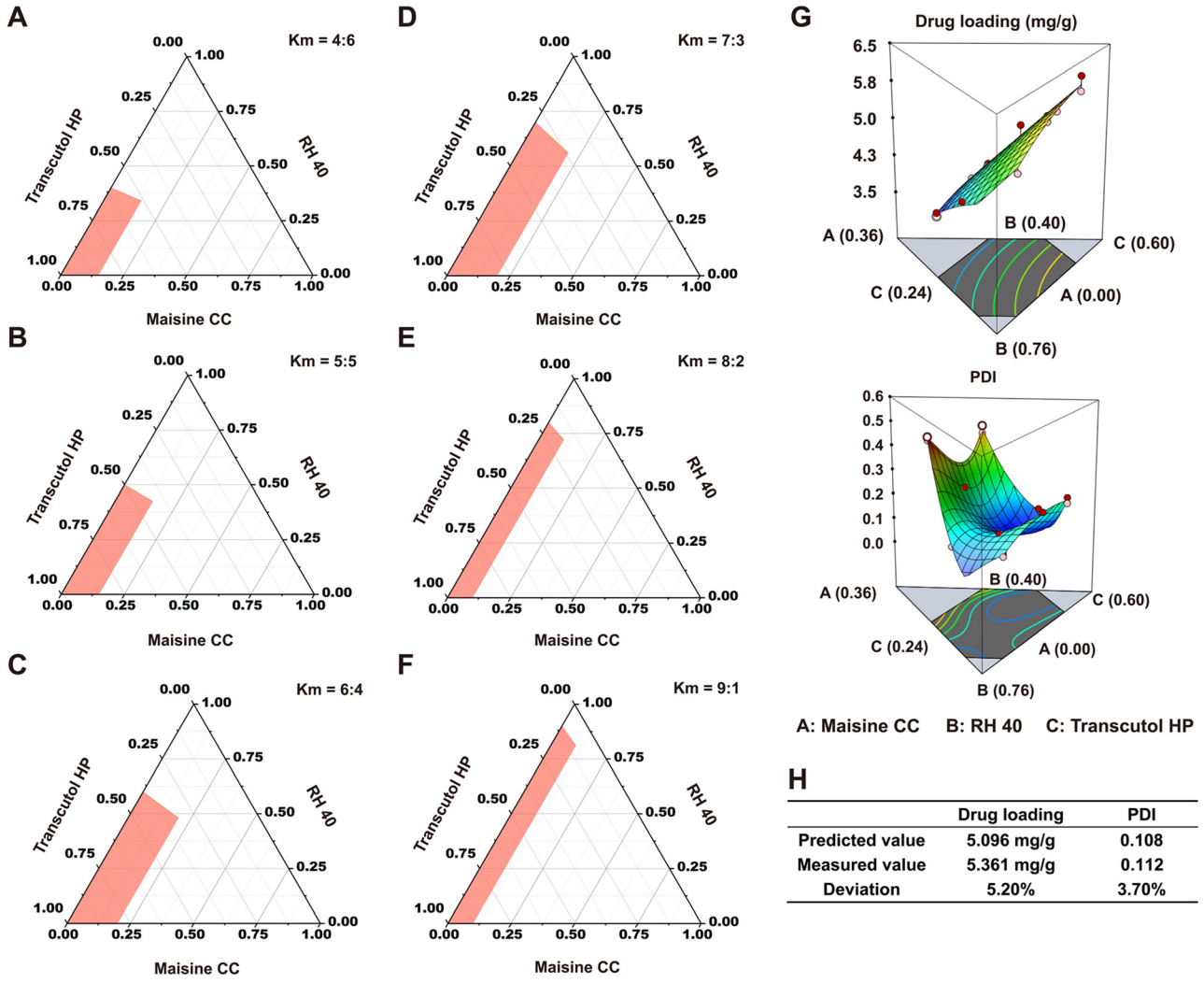

H

	Drug loading	PDI
Predicted value	5.096 mg/g	0.108
Measured value	5.361 mg/g	0.112
Deviation	5.20%	3.70%

Fig. 2 Optimization of SEDDS using Design of Experiments (DOE). (A–F) The ternary phase diagrams of oil phases, surfactant, and co-surfactant with different K_m values (the clear solution forming area is marked). (G) The response surfaces three-dimensional maps of the formulation and indicators. (H) Confirmation of the predicted best formulation.

3.2. Preparation and characterization of MOMIPP-SEDDS

The MOMIPP-SEDDS preconcentrate was prepared by mixing MOMIPP with the optimized SEDDS formulation comprising Maisine® CC, RH 40, and Transcutol® HP at a ratio of 0.1 : 0.429 : 0.471. After emulsification, the MOMIPP-SEDDS had a particle size of 13.97 ± 0.55 nm with a low PDI of 0.11 ± 0.04, and a zeta potential of −3.48 ± 0.23 mV (Fig. 3B and C), classifying it as a self-nanoemulsifying drug delivery system (SNEDDS).[14] Prior to gastrointestinal absorption, SEDDS must overcome the mucus layer barrier to reach the underlying epithelial cells. The interwoven mucus layer creates a microstructure with a mesh pore size of ~10–200 nm that blocks the penetration of large particles.[13] The small particle size affords MOMIPP-SEDDS the potential for crossing the mucus layer. Besides readily accessing the epithelia, the small particle size could allow MOMIPP-SEDDS to be preferentially taken up *via* lymphatic vessels.[31] The morphology of MOMIPP-SEDDS observed by TEM (Fig. 3A) showed spherical particles, and the size was consistent with that measured by dynamic light scattering (DLS, Fig. 3B). The stability of the MOMIPP-SEDDS was also investigated. Eight hours post emulsification, the particle size of the MOMIPP-SEDDS exhibited almost no change (Fig. S1†), indicating a stable small size feature within the time frame of gastrointestinal transport. Additionally, the solution remained clear and transparent with no drug precipitation. The storage stability of the MOMIPP-SEDDS preconcentrate was also investigated under various conditions. Kept at 4 °C, 25 °C, and 60 °C, the MOMIPP-SEDDS preconcentrate was sampled for drug content and self-emulsification behavior examination at predetermined time intervals. The results demonstrated that the drug content in the preconcentrate stored at 60 °C for 30 days slightly dropped to around 90% (Fig. 3E). Nevertheless, no drug crystals were observed in any of the samples using a polarizing microscope. To investigate whether long-term storage could influence the self-emulsification behavior of the preconcentrate, the particle size and the PDI of emulsified MOMIPP-SEDDS were characterized. There were almost no changes in particle size and PDI (Fig. 3F). The storage stability results showed that the MOMIPP-SEDDS preconcentrate maintained a good state under the abovementioned storage conditions.

3.3. *In vitro* drug release behavior

The *in vitro* drug release profiles of MOMIPP-SEDDS and MOMIPP suspensions are depicted in Fig. 3D. The MOMIPP-SEDDS showed a rapid and more complete drug release, with 87.20 ± 1.50% of MOMIPP being released within 12 h, indicating a sustained release of MOMIPP from MOMIPP-SEDDS. However, only 9.12 ± 1.30% of MOMIPP was released from MOMIPP suspensions during the same time. As both formulations reached the plateau phase after 24 h, a much more complete drug release from MOMIPP-SEDDS (98.11 ± 0.68%) was observed, which was around 9.1-fold higher than that from MOMIPP suspensions (10.76 ± 0.02%). Given that the drug release profiles were characterized using a dialysis bag method, the actual drug release *in vivo* might be

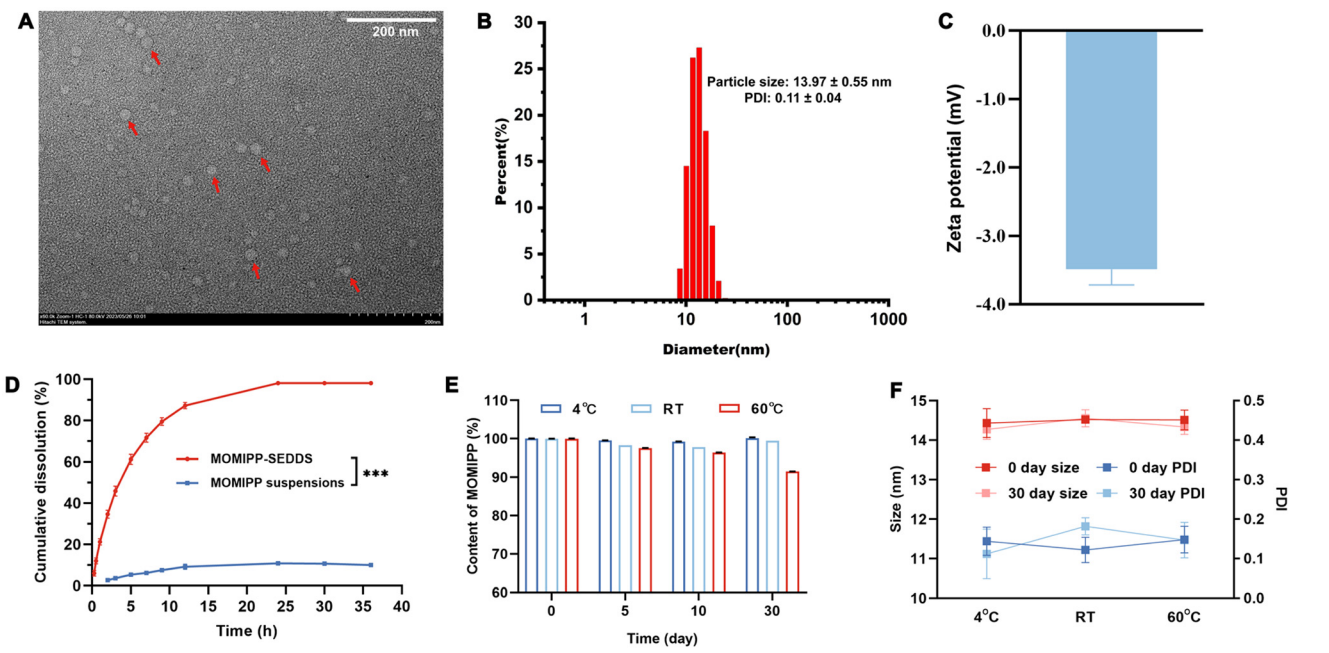

Fig. 3 Characterization of MOMIPP-SEDDS. (A) The morphology of MOMIPP-SEDDS observed by TEM. (B) The particle size distribution of emulsified MOMIPP-SEDDS droplets. (C) The zeta potential of emulsified MOMIPP-SEDDS droplets. (D) The drug release profiles of MOMIPP-SEDDS and MOMIPP suspensions in PBS containing 2% SDS. (E) The changes in MOMIPP content of MOMIPP-SEDDS preconcentrate stored at various temperatures over time. (F) The particle size and PDI of emulsified MOMIPP-SEDDS preconcentrate stored at different temperatures over time. Scale bar = 200 nm. Statistical analysis was performed using *t*-test to compare MOMIPP-SEDDS and MOMIPP suspensions (*p < 0.05, **p < 0.01, and ***p < 0.001).

further enhanced as bile acids and phospholipids form micelles with the SEDDS excipients. Additionally, the permeation-enhancing effect of the SEDDS excipients may also promote drug absorption.[32]

3.4. Cytotoxicity studies

To test the biosafety, the cytotoxicity of blank SEDDS was evaluated on Caco-2 and MDCK cells using MTT assays. López-García *et al*. proposed that cell viability above 80% was considered non-cytotoxic, within 80–60% as weakly cytotoxic, within 60–40% as moderately cytotoxic, and below 40% as strongly cytotoxic.[33] As shown in Fig. 4A, blank SEDDS elicited no apparent cytotoxic impact on Caco-2 or MDCK cells at all concentrations tested (0.25%, 0.1%, 0.05%, 0.01%, v/v). The low cytotoxicity might be attributed to the formulation components, which contain no cationic or anionic surfactants. In actual intestine conditions, the epithelia could be less sensitive to irritation by the SEDDS, owing to the protection from the mucus layer and the tight epithelial structure.[16]

A dose-dependent toxicity study of MOMIPP-SEDDS was conducted to ensure cell viability in cell monolayers during drug transport experiments. Various concentrations of MOMIPP-SEDDS were incubated with Caco-2 and MDCK cells for 4 h (equivalent time with cell monolayer transport). The survival rates of both cells were above 80% at all drug concentrations tested (400, 200, 100, 50, 10, and 5 μM, MOMIPP). The results indicated that MOMIPP-SEDDS were safe for Caco-2 and MDCK cells (Fig. 4B). As for cell monolayers, cells are closely stuck together with tight junctions, where cell viability could be less affected. The images taken by optical microscopy demonstrated that MOMIPP-SEDDS delayed vacuolization formation in Caco-2 cells, indicating enhanced oral administration safety (Fig. 4C and D).

3.5. Cellular uptake and internalization mechanisms of COU-SEDDS

Coumarin 6, as a hydrophobic model drug, was loaded in the SEDDS to track its cellular uptake.[34] As shown in Fig. 5A, the green fluorescence demonstrated that the COU-SEDDS entered the Caco-2 cells readily. The quantitative results determined by flow cytometry showed that the SEDDS endocytosis was a time-dependent process (Fig. 5B), reaching a plateau after 2 h incu-

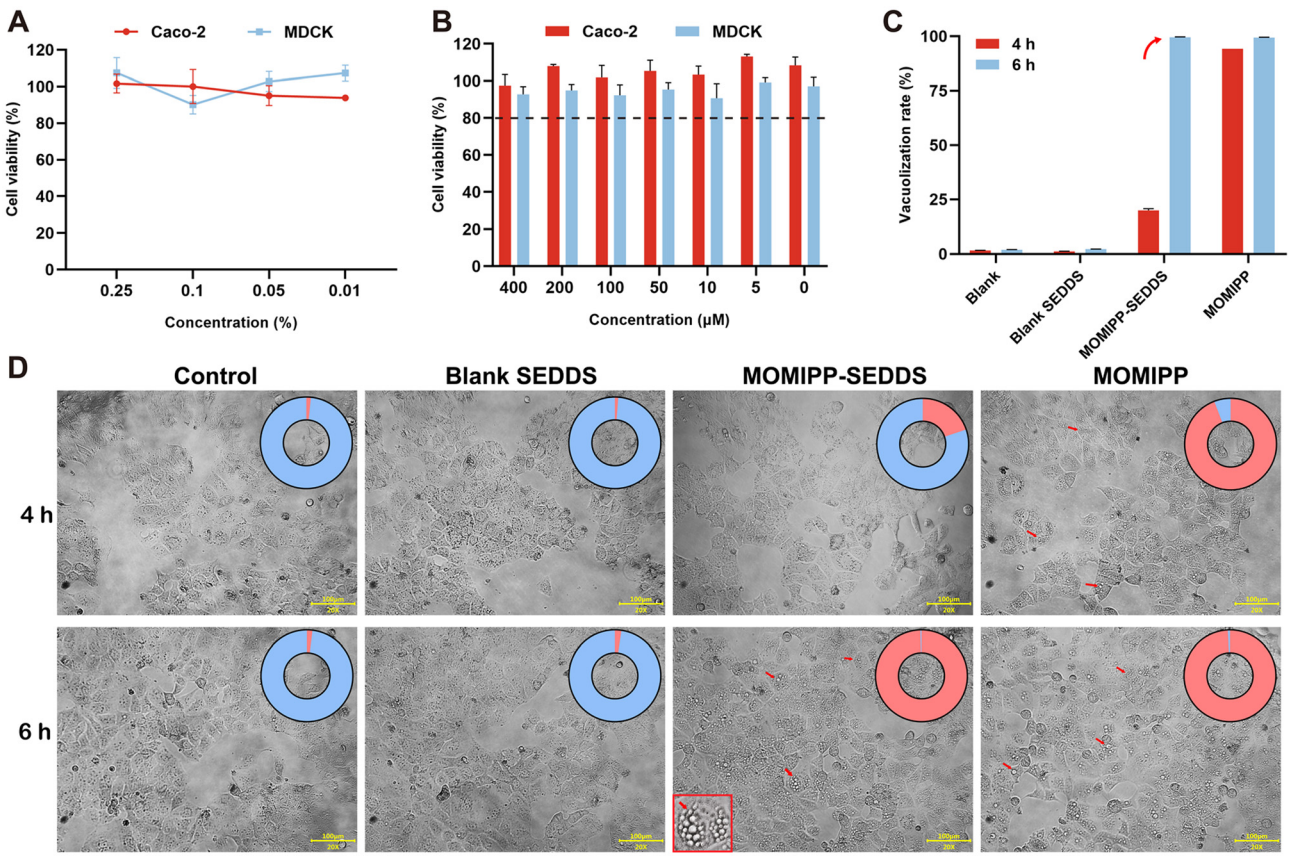

Fig. 4 Cytotoxicity of blank SEDDS and MOMIPP-SEDDS, and the morphological changes of Caco-2 cells. (A) Caco-2 and MDCK survival rates after incubation with various concentrations of blank SEDDS for 24 h. (B) Caco-2 and MDCK cell viability after incubation with various concentrations of MOMIPP-SEDDS for 4 h. The vacuolization rates (C) and the morphological changes (D) of Caco-2 cells after being incubated with DMEM, blank SEDDS, MOMIPP-SEDDS, MOMIPP, and DMSO for 4 h and 6 h. The arrows point out the vacuoles in the cytoplasm, while the inserted panel in the MOMIPP-SEDDS treatment group (6 h) depicts a representative vacuolized cell. Scale bar = 100 μm. The red/blue color represents the ratio of the vacuolized/unvacuolized cells.

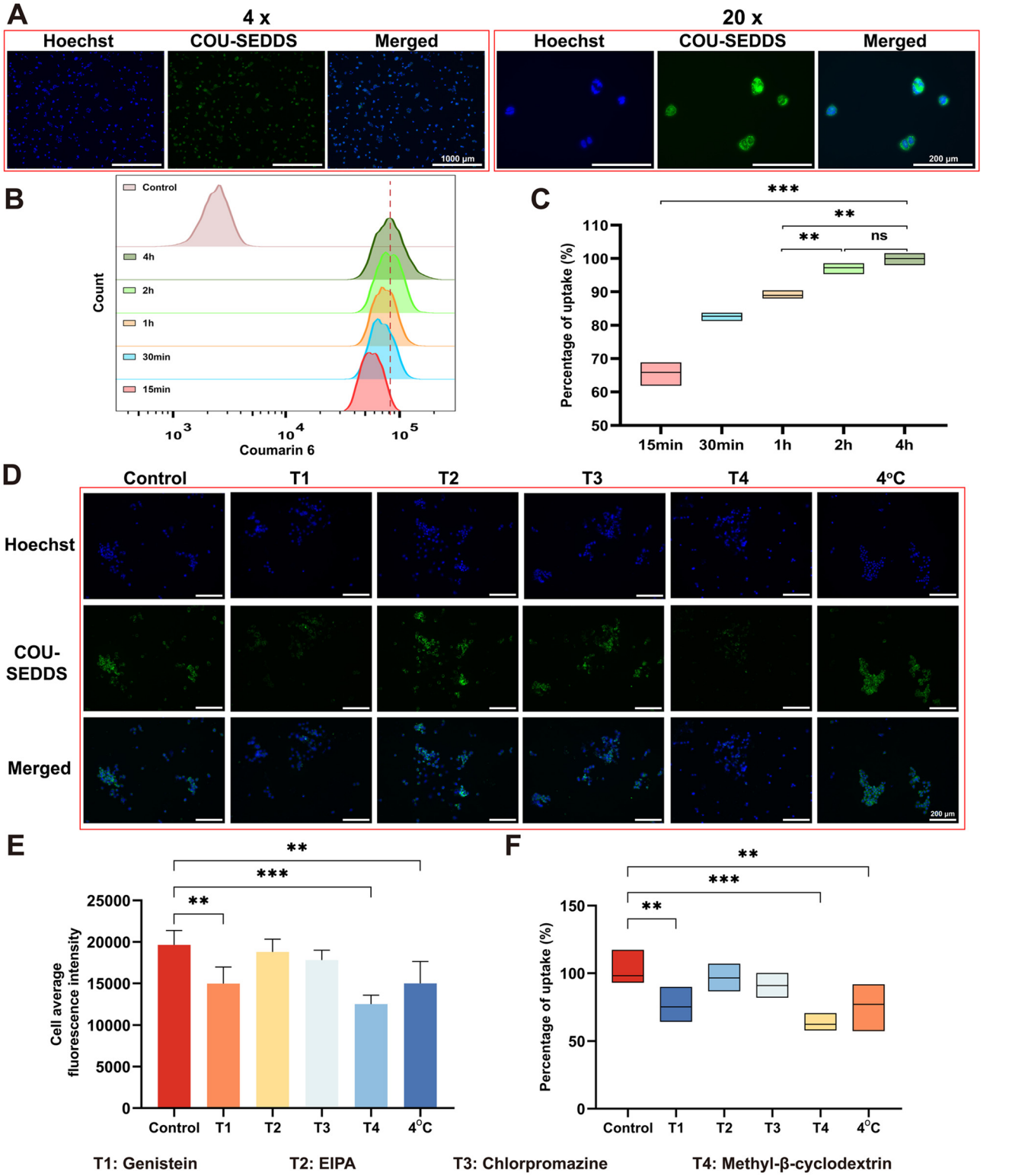

Fig. 5 Cellular uptake and endocytosis mechanisms of the COU-SEDDS. (A) The fluorescence images of Caco-2 cells uptaking COU-SEDDS; (B) coumarin 6 uptake quantified by flow cytometry over time; (C) the relative percentage of cells that took up COU-SEDDS. (D) The fluorescence images of Caco-2 cells uptaking COU-SEDDS in the presence of various inhibitors or low temperature. (E) Fluorescence intensity measured using a high-content imaging system. (F) The relative percentage of cells that took up COU-SEDDS. The scale bar represents 1000 μm in (A) (4×) and 200 μm in (A) (20×) and (D). Statistical analysis was performed using one-way ANOVA with multiple comparisons (*$p < 0.05$, **$p < 0.01$, and ***$p < 0.001$).

bation. From the perspective of relative mean fluorescence intensity (RMFI), COU-SEDDS showed a cellular uptake of 97.23 ± 1.68% at the 2 h time point (Fig. 5C). The fast cellular uptake could promote the SEDDS to enter the enterocytes and prevent SEDDS from being cleared with mucus turnover, benefiting effective intestinal absorption.

To gain a better insight into the endocytosis mechanisms of the nano-sized SEDDS emulsion, the Caco-2 cells were incubated with COU-SEDDS in the presence of various endocytosis inhibitors. As indicated by the decrease in average green fluorescence intensity, the cholesterol depletion agent M-β-CD accounted for 36.1% of uptake reduction, while the tyrosine kinase inhibitor genistein was responsible for 23.6% of endocytosis (Fig. 5D–F). During the internalization, the lipid raft/caveolae pathway played a key role. Moreover, the internalization results of the COU-SEDDS showed partial temperature dependency as the uptake of COU-SEDDS decreased at 4 °C, implying an energy-dependent process.

3.6. Transport of MOMIPP-SEDDS and MOMIPP suspensions across Caco-2 and MDCK cell monolayers

The Caco-2 cell monolayer, similar to enterocytes in morphology and function, has been widely used as an *in vitro* human intestinal epithelium surrogate to investigate drug absorption. When cultured on an insert permeable membrane for 21 days, Caco-2 cells spontaneously differentiate and form apical and basolateral sides with tight junctions and a brush border. Once the Caco-2 cell monolayer was completely formed, the culture medium was replaced with blank HBSS containing MOMIPP-SEDDS (400 μM MOMIPP) to evaluate the transport features. After 4 h of incubation, the amount of MOMIPP transported from the apical side to the basolateral side was determined. Approximately 0.96% of MOMIPP was transported in the MOMIPP-SEDDS group (Fig. 6B). Due to the narrower tight junctions and the higher TEER,[35] the Caco-2 cell monolayer might be harder to cross for drugs or their carriers compared to human intestinal epithelia. Additionally, the carriers and transporters expressed on the Caco-2 cell surfaces differ from those in human intestines.[36] Therefore, to evaluate the transport features of MOMIPP-SEDDS more comprehensively, the amount of transported MOMIPP was further determined using the MDCK cell monolayer model. Approximately a two-fold amount of MOMIPP (1.88%) was transported compared to that in the Caco-2 cell monolayer model (Fig. 6C). Notably, in stark contrast, no MOMIPP was detected on the basolateral side in the MOMIPP suspensions group in either the Caco-2 or MDCK cell monolayer model. Collectively, our findings confirmed that the SEDDS notably promoted the transport of MOMIPP across Caco-2 and MDCK cell monolayers, indicating that MOMIPP-SEDDS may have better *in vivo* absorption.

3.7. Intestinal absorption of MOMIPP-SEDDS and MOMIPP suspensions using an *ex vivo* everted gut sac

Although the MOMIPP-SEDDS exhibited superior absorption of water-insoluble MOMIPP across the cell monolayer, the enterocyte barrier in the intestine and the mucus layer lying on the epithelium are two major barriers that drugs must cross. Since neither of the cell monolayer models used in this study can form a mucus layer, an *ex vivo* everted gut sac was employed to better simulate the absorption situations. The absorbing section of the everted sac was immersed in the K–R bicarbonate solution containing emulsified MOMIPP-SEDDS or MOMIPP suspensions (equivalent to 400 μM MOMIPP). As shown in Fig. 6D, the transport of MOMIPP across the everted gut sac increased over time. By the 2 hour time point, a total amount of 1.89 ± 0.19 μg MOMIPP was absorbed per 10 cm gut sac section in the MOMIPP-SEDDS group, while no detectable drug was observed in the MOMIPP suspensions group. These findings were consistent with the results demonstrated in cell monolayer permeation, both indicating that the absorption of MOMIPP was significantly enhanced by the SEDDS. All these results laid a good foundation for effective MOMIPP *in vivo* delivery.

3.8. *In vivo* pharmacokinetic studies

Inspired by the impressive absorption performance of MOMIPP-SEDDS *in vitro* and *ex vivo*, the pharmacokinetics profiles, especially the absorption of MOMIPP, were investigated in rats. The rats were randomly divided into two groups and administered MOMIPP-SEDDS (50 mg kg^{-1}, MOMIPP) and MOMIPP suspensions (50 mg kg^{-1}, MOMIPP), respectively. As illustrated in Fig. 6E and F, significant increases in pharmacokinetic parameters were seen in the MOMIPP-SEDDS group. The mean residence time of MOMIPP was prolonged from 3.47 h to 4.69 h. Furthermore, the C_{max} of MOMIPP-SEDDS was 1296.20 ± 190.45 ng mL^{-1}, much higher than that of MOMIPP suspensions (97.13 ± 20.63 ng mL^{-1}). Correspondingly, the area under the curve (AUC) value of MOMIPP-SEDDS increased by 19.98 times (7576.99 ± 2543.74 μg h L^{-1}) compared with that of MOMIPP suspensions (360.99 ± 184.17 μg h L^{-1}). The striking enhancement in MOMIPP absorption in rats validated the superiority of MOMIPP-SEDDS. Additionally, a second peak was shown in the plasma concentration-time curve in the MOMIPP-SEDDS group. It might be the unique feature of SEDDS formulation because no second peak was observed in the MOMIPP suspensions group. The appearance of a remarkable increase in AUC found in MOMIPP-SEDDS might be the result of the promoted lymphatic transport.[19,37] In the enterocytes, the drug could be released as free molecules or bind to the chylomicrons for lymphatic transport, thus prominently enhancing the oral absorption of MOMIPP and increasing its bioavailability.

3.9. *In vivo* tumor inhibition

Encouraged by the enhanced oral bioavailability, the *in vivo* antitumor efficacy of MOMIPP-SEDDS was evaluated in a xenograft tumor model (HeLa cells). The results demonstrated that oral administration of MOMIPP-SEDDS achieved obvious tumor inhibition, with the tumor volumes shrinking to half

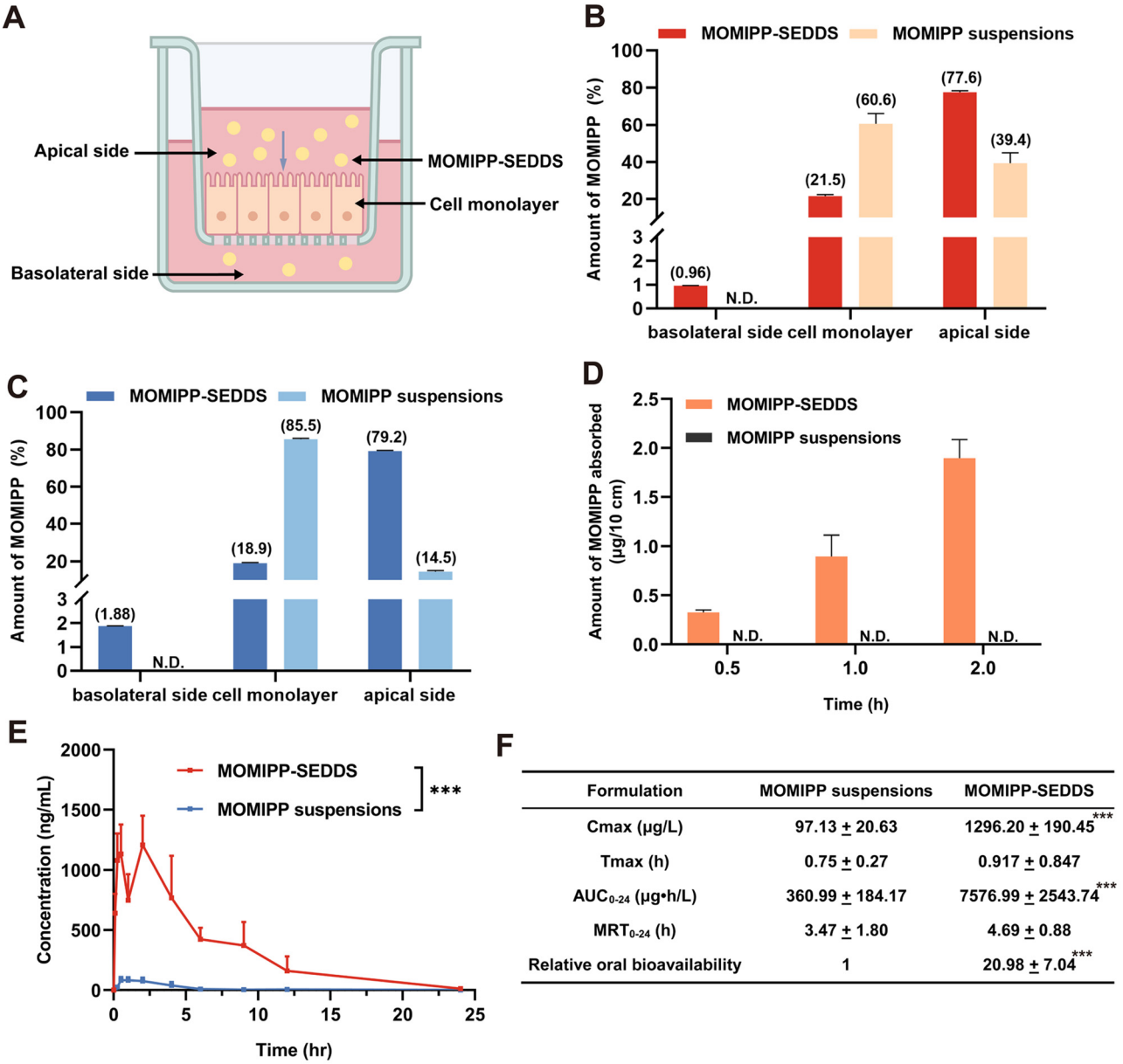

Formulation	MOMIPP suspensions	MOMIPP-SEDDS
Cmax (μg/L)	97.13 ± 20.63	1296.20 ± 190.45***
Tmax (h)	0.75 ± 0.27	0.917 ± 0.847
AUC_{0-24} (μg•h/L)	360.99 ± 184.17	7576.99 ± 2543.74***
MRT_{0-24} (h)	3.47 ± 1.80	4.69 ± 0.88
Relative oral bioavailability	1	20.98 ± 7.04***

Fig. 6 The MOMIPP-SEDDS enhanced oral drug absorption. (A) Schematic diagram of drug transport across the cell monolayers. (B) The amount of transported MOMIPP crossing the Caco-2 cell monolayer. (C) The amount of transported MOMIPP across the MDCK cell monolayer. (D) The amount of MOMIPP absorbed in the everted gut sac. (E) The plasma concentration-time curves in rats determined using UPLC-MS/MS. (F) The corresponding pharmacokinetic parameters of MOMIPP. Statistical analysis was performed using *t*-test to compare MOMIPP-SEDDS and MOMIPP suspensions (*p < 0.05, **p < 0.01, and ***p < 0.001). Samples with a drug concentration below the detectable level are marked as N.D.

size (Fig. 7C and E). The decent tumor growth inhibition rate (47.5%) also verified the efficacy of MOMIPP-SEDDS (Fig. 7D). Although the blank SEDDS and the MOMIPP suspensions seemed to have slight antitumor effects, neither exhibited a significant difference in tumor volume or weight (Fig. 7C and F). The results of Ki67 staining confirmed that MOMIPP-SEDDS retarded the progression of cancer cell proliferation (Fig. 8). Additionally, a significant vacuolization phenomenon was found in tumor ultrathin sections from the MOMIPP-SEDDS treatment group, confirming the tumor inhibition mediated by the methuosis of MOMIPP (Fig. 9). These encouraging pharmacodynamic results suggested the successful oral delivery of the methuosis-inducing compound MOMIPP by the SEDDS with a new-found antitumor mechanism.

3.10. The *in vivo* safety profile

No significant body weight changes were observed throughout the experiment (Fig. 7B). As shown in the H&E staining images of the pathological sections from the major organs, no sys-

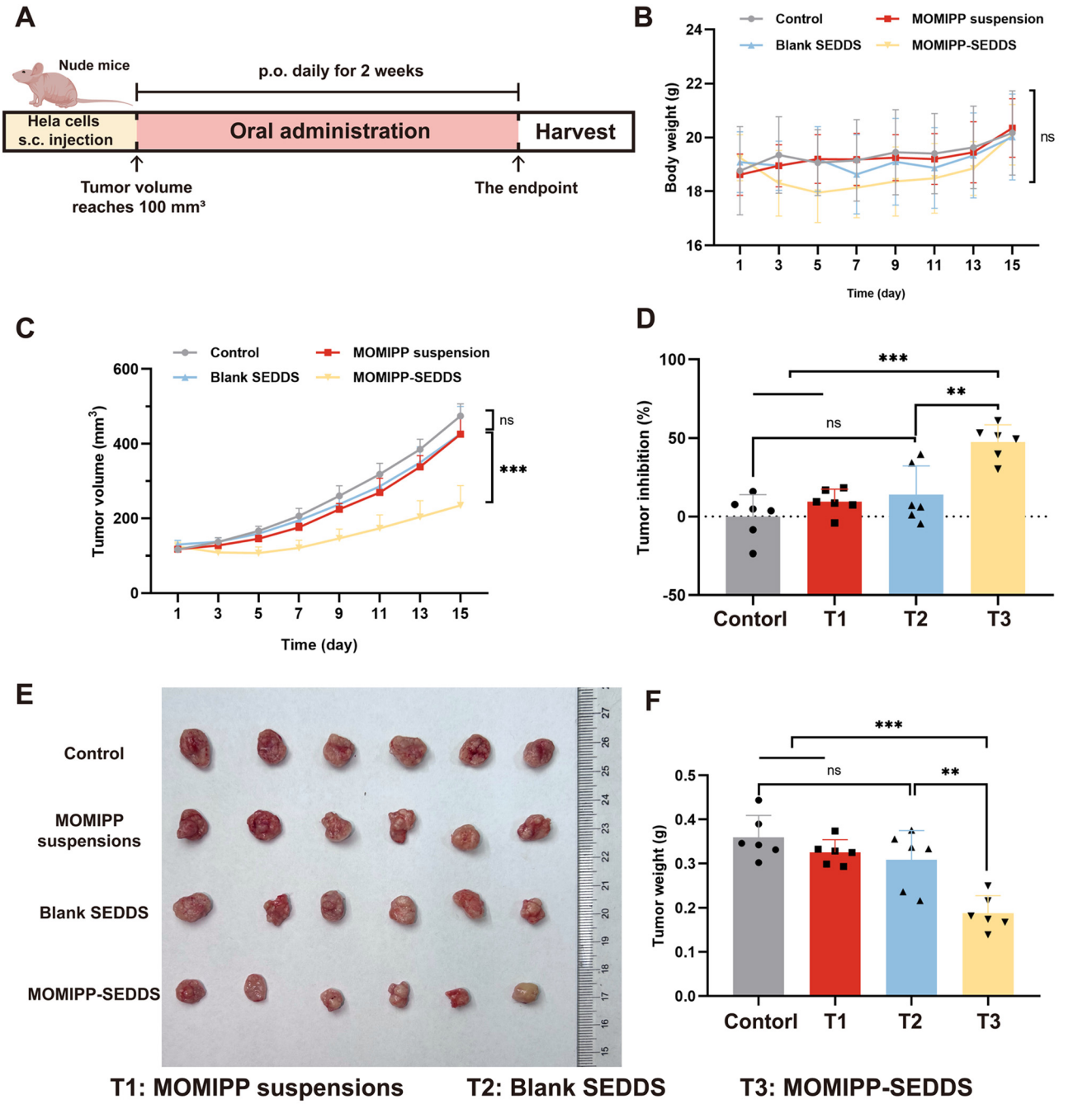

Fig. 7 *In vivo* antitumor efficacy of MOMIPP-SEDDS in balb/c-nu mice. (A) Schematic diagram of tumor model establishment and treatment regimen. (B) The body weight changes throughout the treatment. (C) The tumor volume variations during the treatment. (D) The tumor inhibition rates calculated at the endpoint. (E) The dissected tumor picture at the endpoint. (F) The tumor weights at the endpoint. Statistical analysis was performed using one-way ANOVA with multiple comparisons (*$p < 0.05$, **$p < 0.01$, and ***$p < 0.001$).

temic toxicity was found, indicating the safe oral administration of MOMIPP-SEDDS (Fig. 10). Additionally, the histopathological conditions of the jejunum were specifically examined, as the jejunum plays an important absorbing role in the intestine. Similarly, oral administration of MOMIPP-SEDDS for 14 consecutive days caused no obvious tissue damage to the jejunum.

4. Discussion

Due to the vulnerability of apoptosis-regulating genes to mutations, traditional antitumor drugs face increasingly severe resistance issues. Therefore, seeking other potential alternatives to induce cancer cell death is an important strategy for cancer treatment. Chemotherapies relying on non-apoptotic

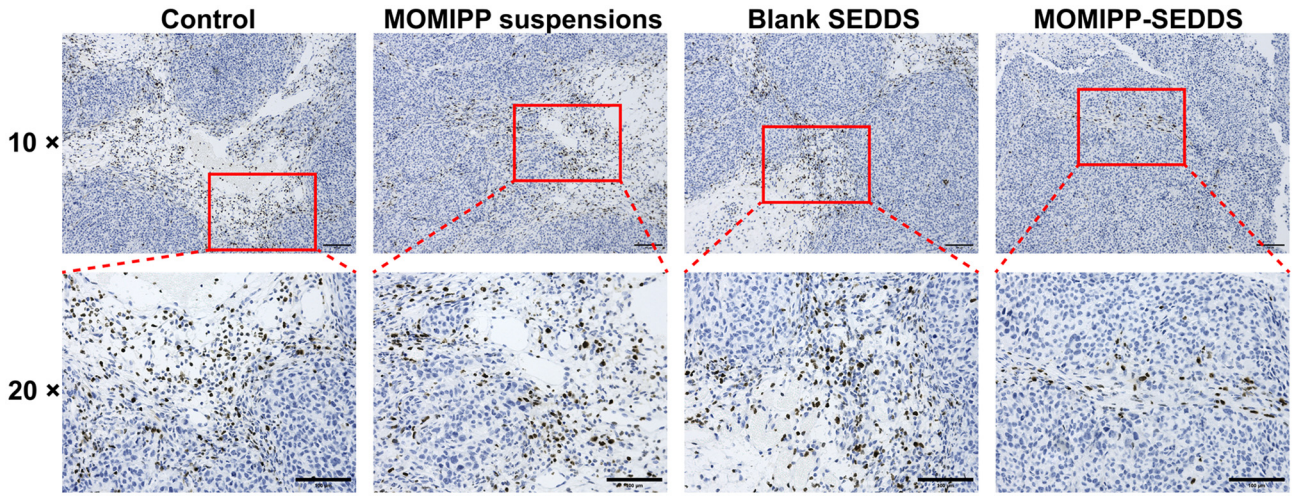

Fig. 8 Immunohistochemistry of the tumor sections was performed using antibodies for Ki67 staining after treatment. Scale bar = 100 μm.

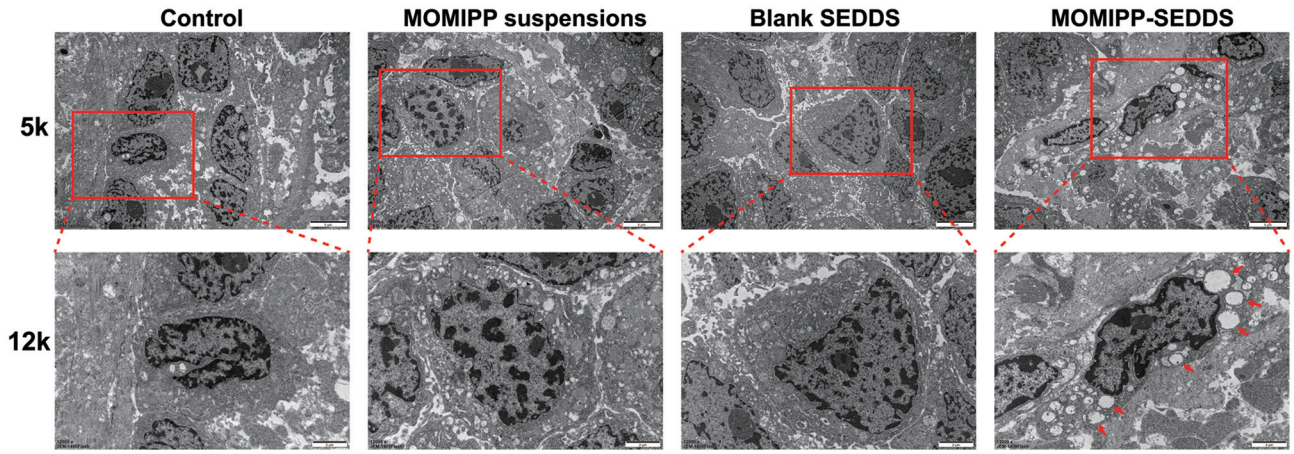

Fig. 9 Representative transmission electron microscopy images of dissected tumor tissues after treatment. The arrows point at the vacuoles in the cytoplasm. Scale bar = 5 μm (5000×), = 2 μm (12 000×).

mechanisms have aroused significant research interest. Methuosis induces cancer cell death in a caspase-independent manner with a novel non-apoptotic mechanism, characterized by large vacuoles in the cytoplasm. Although the iconic methuosis-inducer, MOMIPP, exhibits attractive cytotoxic effects on some cancer cell lines (especially on TMZ-resistant U251 and Dox-resistant MCF-7 cells), its poor solubility in most solvents and unsatisfactory pharmacokinetic properties hinder its further dosing in animals to verify the *in vivo* antitumor efficacy. This issue poses great challenges to pharmaceutical scientists in developing efficient drug delivery systems for MOMIPP. Attempts have been made to deliver MOMIPP by intravenous and intraperitoneal injections.[9,10,12] However, injections bring issues of low compliance and inconvenience for patients. Additionally, the therapeutic effectiveness of reported MOMIPP formulations at the animal level was not well verified through these means of administration.

To the best of our knowledge, the self-emulsifying drug delivery system reported here is the first effective carrier designed for the oral delivery of MOMIPP and achieves a favorable therapeutic antitumor effect *in vivo*. The limited types of solvents available for selection restrict the routes of MOMIPP delivery to a large degree. Therefore, our strategy was switched to the oil phase for enhancing MOMIPP solubility and we surprisingly found a potential solution to deliver MOMIPP orally. By screening SEDDS excipients and optimizing formulations *via* DOE, the optimal MOMIPP-SEDDS with acceptable drug solubility and good self-emulsification properties was obtained. The enhanced oral absorption by SEDDS led to an apparent increase in the relative bioavailability of MOMIPP. Of note, MOMIPP-SEDDS demonstrated a valid *in vivo* therapeutic effect on the HeLa xenograft tumor model in mice.

SEDDS is a promising carrier for delivering hydrophobic drugs. With an elaborate experimental design, the optimized

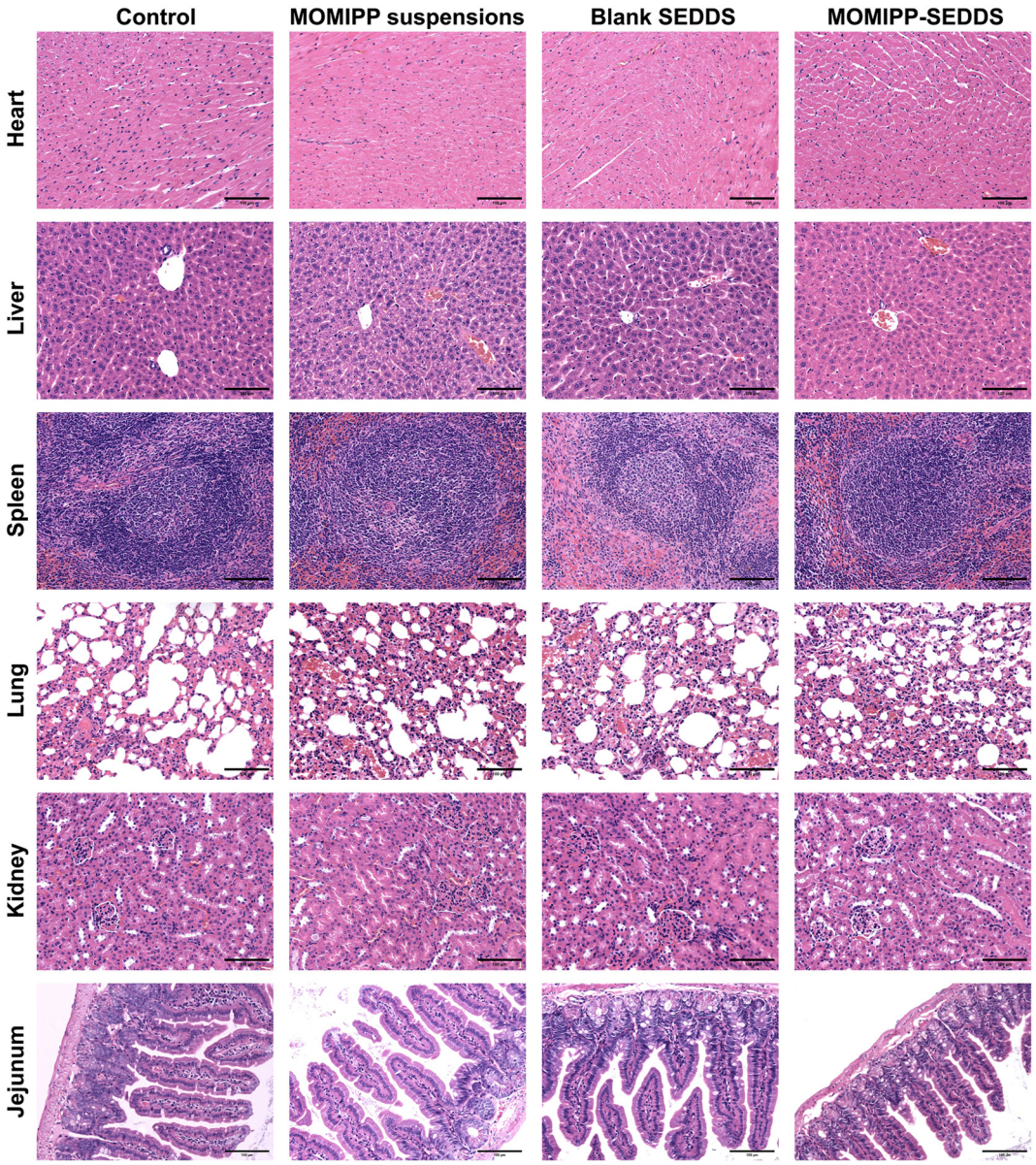

Fig. 10 *In vivo* safety evaluation of the MOMIPP-SEDDS. The representative H&E staining of dissected major organs at the endpoint (heart, liver, spleen, lung, kidney, and jejunum). Scale bar = 100 μm.

MOMIPP-SEDDS remarkably increased the drug concentration and AUC in rat blood. The attribute of enhanced absorption resulted solely from the unique properties of the SEDDS, whereas the MOMIPP suspensions exhibited poor transport of in both cell monolayers and everted gut sacs. Furthermore, the SEDDS loaded with MOMIPP was internalized into Caco-2 cells *via* a lipid raft/caveolae-dependent manner, consistent with another study reported by Jun Ye *et al.*[38] A recent study reported that the IC_{50} value of MOMIPP in HeLa cells was 0.88 ± 0.53 μM, and three hours of MOMIPP treatment at 1 μM could lead to vacuolization in the cytoplasm.[39] Based on our pharmacokinetic data, nude mice were orally dosed with MOMIPP-SEDDS once a day for 2 weeks in the antitumor efficacy study. The reduction in tumor volume and the superior tumor inhibition rate reflected the straightforward therapeutic effects of MOMIPP-SEDDS, and the immunohistochemistry results indicated that MOMIPP-SEDDS efficiently inhibited the proliferation of HeLa cells. Furthermore, the vacuolization in HeLa xenograft tumors from the MOMIPP-SEDDS treatment group was confirmed for the first time using TEM examination on morphology changes.[39,40]

This study provided a first step in delivering MOMIPP through the oral route using SEDDS and proved the therapeutic effectiveness of this classic methuosis inducer *in vivo*. It paved a new direction for tackling the challenges of delivering water-insoluble MOMIPP. Although the tumor inhibition performance was not dramatic, the route of oral administration is ideal for long-term cancer treatment if the biosafety of the

carrier is acceptable and tolerable. With a wider range of accessible excipients, more potent strategies could be expected for efficiently dosing MOMIPP. Since MOMIPP triggers macropinocytosis in certain cell lines, combining other drugs in the SEDDS has great potential in designing synergistic strategies and treating other cancer diseases.

5. Conclusion

In this study, a self-emulsifying drug delivery system was developed to enable the oral delivery of the insoluble methuosis inducer, MOMIPP. MOMIPP was found to induce methuosis in temozolomide-resistant U251 and doxorubicin-resistant MCF-7 cells, indicating its promise in combating refractory tumors through this novel non-apoptotic mechanism. However, the insolubility of MOMIPP in most solvents posed significant challenges in dosing and achieving its therapeutic effects, as no satisfactory *in vivo* antitumor efficacy had been demonstrated since MOMIPP was first reported in 2012. By screening the excipients and optimizing the formulations, a satisfactory MOMIPP-SEDDS was successfully prepared, which remarkably improved the pharmacokinetic properties of MOMIPP. Benefiting from the specially developed SEDDS formulation, MOMIPP-SEDDS increased the relative bioavailability by 19.98-fold and achieved favorable tumor inhibition. Furthermore, clear evidence of methuosis in the tumor tissue following MOMIPP-SEDDS treatment was revealed by TEM imaging. Our findings have substantiated the therapeutic effectiveness of the oral delivery of MOMIPP and opened up a new avenue for delivering methuosis inducers *via* SEDDS. With the further incorporation of other antitumor agents, this oral delivery strategy could hold great potential for a broader range of cancer therapies.

Ethics approval and consent to participate

All animal experiments were conducted in compliance with the guidelines of the National Research Council's Guide for the Care and Use of Laboratory Animals and were performed in accordance with the approved protocols (approval numbers: 2023002636 and 2023003046) and the established guidelines of the Institutional Animal Care and Use Committee of Sun Yat-sen University.

Author contributions

Z. Y. Mao conducted the research, analyzed the data, prepared all figures and tables, and wrote the main manuscript text. G. H. Chai oversaw project administration and supervision, acquired funding, and was responsible for proofreading and revising the manuscript. All authors read and approved the final manuscript.

Data availability

The datasets used and/or analyzed during the current study are available from the corresponding author upon reasonable request.

Conflicts of interest

The authors declare no competing interests.

Acknowledgements

This work was supported by funding from the Guangdong Basic and Applied Basic Research Foundation (No. 2023A1515011064), the Medical Scientific Research Foundation of Guangdong Province (No. A2023090), the Fundamental Research Funds for the Central Universities (No. 22qntd4503), the Open Project of State Key Laboratory of Respiratory Disease (No. SKLRD-OP-202302), and the Open Project of The Key Laboratory of Diagnosis and Treatment of Digestive System Tumors of Zhejiang Province under Award Number 2019E10020 (KFJJ-202202).

References

1 L. H. Hurley, DNA and its associated processes as targets for cancer therapy, *Nat. Rev. Cancer*, 2002, **2**(3), 188–200.
2 F. T. Andón and B. Fadeel, Programmed cell death: molecular mechanisms and implications for safety assessment of nanomaterials, *Acc. Chem. Res.*, 2013, **46**(3), 733–742.
3 F. Lefranc, J. Brotchi and R. Kiss, Possible future issues in the treatment of glioblastomas: special emphasis on cell migration and the resistance of migrating glioblastoma cells to apoptosis, *J. Clin. Oncol.*, 2005, **23**(10), 2411–2422.
4 N. Vasan, J. Baselga and D. M. Hyman, A view on drug resistance in cancer, *Nature*, 2019, **575**(7782), 299–309.
5 M. W. Robinson, J. H. Overmeyer, A. M. Young, *et al.*, Synthesis and evaluation of indole-based chalcones as inducers of methuosis, a novel type of nonapoptotic cell death, *J. Med. Chem.*, 2012, **55**(5), 1940–1956.
6 J. H. Overmeyer, A. Kaul, E. E. Johnson, *et al.*, Active ras triggers death in glioblastoma cells through hyperstimulation of macropinocytosis, *Mol. Cancer Res.*, 2008, **6**(6), 965–977.
7 H. Cho, E. Geno, M. Patoor, *et al.*, Indolyl-pyridinyl-propenone-induced methuosis through the inhibition of PIKFYVE, *ACS Omega*, 2018, **3**(6), 6097–6103.
8 N. E. Mbah, J. H. Overmeyer and W. A. Maltese, Disruption of endolysosomal trafficking pathways in glioma cells by methuosis-inducing indole-based chalcones, *Cell Biol. Toxicol.*, 2017, **33**(3), 263–282.
9 Z. Li, N. E. Mbah, J. H. Overmeyer, *et al.*, The JNK signaling pathway plays a key role in methuosis (non-apoptotic cell death) induced by MOMIPP in glioblastoma, *BMC Cancer*, 2019, **19**(1), 77.

10 F. Oppong, Z. Li, E. A. Fakhrabadi, *et al.*, Investigating the potential to deliver and maintain plasma and brain levels of a novel practically insoluble methuosis inducing anticancer agent 5-methoxy MOMIPP through an injectable in situ forming thermoresponsive hydrogel formulation, *J. Pharm. Sci.*, 2020, **109**(9), 2719–2728.
11 S. M. Abuzar, S.-M. Hyun, J.-H. Kim, *et al.*, Enhancing the solubility and bioavailability of poorly water-soluble drugs using supercritical antisolvent (SAS) process, *Int. J. Pharm.*, 2018, **538**(1), 1–13.
12 K. N. Shah, A. J. Ditto, D. C. Crowder, *et al.*, Receptor-mediated attachment and uptake of hyaluronan conjugates by breast cancer cells, *Mol. Pharm.*, 2017, **14**(11), 3968–3977.
13 M. Arshad and B.-S. Andreas, SEDDS: A game changing approach for the oral administration of hydrophilic macromolecular drugs, *Adv. Drug Delivery Rev.*, 2019, **142**, 91–101.
14 M. Indrani, M. Srushti, S. Anitha, *et al.*, Solid self emulsifying drug delivery system: Superior mode for oral delivery of hydrophobic cargos, *J. Controlled Release*, 2021, **337**, 646–660.
15 M. Claudia, H. Thomas, L. Flavia, *et al.*, In vivo evaluation of an oral self-emulsifying drug delivery system (SEDDS) for exenatide, *J. Controlled Release*, 2018, **277**, 165–172.
16 G. Leonaviciute and B.-S. Andreas, Self-emulsifying drug delivery systems in oral (poly)peptide drug delivery, *Expert Opin. Drug Delivery*, 2015, **12**(11), 1703–1716.
17 M. Kazi, M. Al-Swairi, A. Ahmad, *et al.*, Evaluation of self-nanoemulsifying drug delivery systems (SNEDDS) for poorly water-soluble talinolol: Preparation, in vitro and in vivo assessment, *Front. Pharmacol.*, 2019, **10**, 459.
18 B. Ayesha, A. Rabia, R. Sobia, *et al.*, Formulation and evaluation of hyaluronic acid-based mucoadhesive self nanoemulsifying drug delivery system (SNEDDS) of tamoxifen for targeting breast cancer, *Int. J. Biol. Macromol.*, 2020, **152**, 503–515.
19 Z. Zichen, L. Yi, Q. Jianping, *et al.*, An update on oral drug delivery via intestinal lymphatic transport, *Acta Pharm. Sin. B*, 2021, **11**(8), 2449–2468.
20 A. F. Hofmann, Micellar solubilization of fatty acids and monoglycerides by bile salt solutions, *Nature*, 1961, **190**(4781), 1106–1107.
21 K. S. Kim, K. Suzuki, H. Cho, *et al.*, Oral nanoparticles exhibit specific high-efficiency intestinal uptake and lymphatic transport, *ACS Nano*, 2018, **12**(9), 8893–8900.
22 A. M. Jörgensen, C. Steinbring, D. Stengel, *et al.*, Self-emulsifying drug delivery systems (SEDDS) containing reverse micelles: Advanced oral formulations for therapeutic peptides, *Adv. Healthcare Mater.*, 2023, **12**(31), 2302034.
23 A. J. Coupe, S. S. Davis and I. R. Wilding, Variation in gastrointestinal transit of pharmaceutical dosage forms in healthy subjects, *Pharm. Res.*, 1991, **8**(3), 360–364.
24 J. N. Chu and G. Traverso, Foundations of gastrointestinal-based drug delivery and future developments, *Nat. Rev. Gastroenterol. Hepatol.*, 2022, **19**(4), 219–238.
25 A. M. Bannunah, D. Vllasaliu, J. Lord, *et al.*, Mechanisms of nanoparticle internalization and transport across an intestinal epithelial cell model: Effect of size and surface charge, *Mol. Pharm.*, 2014, **11**(12), 4363–4373.
26 G.-H. Chai, Y. Xu, S.-Q. Chen, *et al.*, Transport mechanisms of solid lipid nanoparticles across Caco-2 cell monolayers and their related cytotoxicology, *ACS Appl. Mater. Interfaces*, 2016, **8**(9), 5929–5940.
27 P. Khatri and J. Shao, Impact of digestion on the transport of dextran-loaded self-emulsified nanoemulsion through MDCK epithelial cell monolayer and rat intestines, *Int. J. Pharm.*, 2018, **536**(1), 353–359.
28 P. Chen, M. Zhao, Q. Chen, *et al.*, Absorption characteristics of chitobiose and chitopentaose in the human intestinal cell line Caco-2 and everted gut sacs, *J. Agric. Food Chem.*, 2019, **67**(16), 4513–4523.
29 H. Yuan, C.-Y. Chen, G.-H. Chai, *et al.*, Improved transport and absorption through gastrointestinal tract by PEGylated solid lipid nanoparticles, *Mol. Pharm.*, 2013, **10**(5), 1865–1873.
30 K. Jun Hyeok, O. Dong Hoon, O. Yu-Kyoung, *et al.*, Effects of solid carriers on the crystalline properties, dissolution and bioavailability of flurbiprofen in solid self-nanoemulsifying drug delivery system (solid SNEDDS), *Eur. J. Pharm. Biopharm.*, 2012, **80**(2), 289–297.
31 D. Wang, Q. Jiang, Z. Dong, *et al.*, Nanocarriers transport across the gastrointestinal barriers: The contribution to oral bioavailability via blood circulation and lymphatic pathway, *Adv. Drug Delivery Rev.*, 2023, **203**, 115130.
32 F. Hintzen, F. Laffleur, F. Sarti, *et al.*, In vitro and ex vivo evaluation of an intestinal permeation enhancing self-microemulsifying drug delivery system (SMEDDS), *J. Drug Delivery Sci. Technol.*, 2013, **23**(3), 261–267.
33 J. López-García, M. Lehocký, P. Humpolíček, *et al.*, HaCaT keratinocytes response on antimicrobial atelocollagen substrates: Extent of cytotoxicity, cell viability and proliferation, *J. Funct. Biomater.*, 2014, **5**(2), 43–57.
34 B. He, P. Lin, Z. Jia, *et al.*, The transport mechanisms of polymer nanoparticles in Caco-2 epithelial cells, *Biomaterials*, 2013, **34**(25), 6082–6098.
35 A. Béduneau, C. Tempesta, S. Fimbel, *et al.*, A tunable Caco-2/HT29-MTX co-culture model mimicking variable permeabilities of the human intestine obtained by an original seeding procedure, *Eur. J. Pharm. Biopharm.*, 2014, **87**(2), 290–298.
36 K. E. Samy, E. S. Levy, K. Phong, *et al.*, Human intestinal spheroids cultured using sacrificial micromolding as a model system for studying drug transport, *Sci. Rep.*, 2019, **9**(1), 9936.
37 N. L. Trevaskis, W. N. Charman and C. J. H. Porter, Lipid-based delivery systems and intestinal lymphatic drug transport: A mechanistic update, *Adv. Drug Delivery Rev.*, 2008, **60**(6), 702–716.
38 J. Ye, Y. Gao, M. Ji, *et al.*, Oral SMEDDS promotes lymphatic transport and mesenteric lymph nodes target of chlorogenic acid for effective T-cell antitumor immunity, *J. Immunother. Cancer*, 2021, **9**(7), e002753.

39 Y. Chen, S. Liu, Y. Wei, *et al.*, Discovery of potent and selective phosphatidylinositol 3-phosphate 5-kinase (PIKfyve) inhibitors as methuosis inducers, *J. Med. Chem.*, 2024, **67**(1), 165–179.

40 L. Sun, B. Li, X. Su, *et al.*, An ursolic acid derived small molecule triggers cancer cell death through hyperstimulation of macropinocytosis, *J. Med. Chem.*, 2017, **60**(15), 6638–6648.